Dissecting the Inner Galaxy with γ-Ray Pixel Count Statistics

F. Calore,[1,*] F. Donato,[2,3,†] and S. Manconi[4,‡]
[1]Université Grenoble Alpes, USMB, CNRS, LAPTh, F-74940 Annecy, France
[2]Dipartimento di Fisica, Università di Torino, via P. Giuria, 1, I-10125 Torino, Italy
[3]Istituto Nazionale di Fisica Nucleare, Sezione di Torino, via P. Giuria, 1, I-10125 Torino, Italy
[4]Institute for Theoretical Particle Physics and Cosmology, RWTH Aachen University, Sommerfeldstraße 16, 52056 Aachen, Germany

(Received 4 March 2021; revised 11 May 2021; accepted 3 September 2021; published 13 October 2021)

We combine adaptive template fitting and pixel count statistics in order to assess the nature of the Galactic Center excess in Fermi-LAT data. We reconstruct the flux distribution of point sources well below the Fermi-LAT detection threshold, and measure their radial and longitudinal profiles in the inner Galaxy. We find that all point sources *and* the bulge-correlated diffuse emission each contributes $\mathcal{O}(10\%)$ of the total inner Galaxy emission, and disclose a potential subthreshold point-source contribution to the Galactic Center excess.

DOI: 10.1103/PhysRevLett.127.161102

Introduction.—The Galactic Center excess (GCE) shows up as an unexpected γ-ray component in the data of the Large Area Telescope (LAT), aboard the Fermi satellite, at GeV energies, from the inner degrees of the Galaxy [1–5]. Despite the great interest raised by the GCE discovery, its nature is still unknown. While the GCE morphology has been found to be consistent with a Navarro, Frenk, and White (NFW) profile [6] for annihilating particle dark matter (DM) in [1,4,7–10], it could also be due to a population of millisecond pulsars, as proposed by [11]. Stellar distributions were used as tracers of point sources (PS) emitting below threshold, and turned out to match the morphological features of GCE photons better than DM-inspired templates in [12–14]. All these results were obtained by γ-ray analyses based on the, so-called, template fitting. In parallel, complementary methods, based on photon-count statistics and aimed at detecting new point sources below the threshold of the Fermi catalogs were developed. They initially revealed that the GCE can be entirely due to a population of PS [15,16]. More recently, the DM interpretation was brought back by [17], although hampered by systematics affecting photon-count statistical methods [18–22]. Techniques involving neural networks have also been explored [23,24]. As a conclusive probe of the PS nature of the GCE, a fully multiwavelength approach has been proposed, from radio to gravitational wave observations [25–27].

A major limitation to all these studies is the modeling of the Galactic diffuse foreground, and the impact of residual mismodeled emission on the results' robustness. As for template fitting methods, the analysis of the diffuse emission has been recently approached with the `skyFACT` algorithm, which fits the γ-ray sky by combining methods of image reconstruction and adaptive spatial and spectral template regression [28]. The `skyFACT` method has been tested in the *inner Galaxy* (IG) region, and probed to be efficient in the removal of most residual emission for a robust assessment of the GCE properties [12,28]. Another source of uncertainty is the contribution of subthreshold PSs. Photon-count statistical methods can discriminate photons from γ-ray sources based on their statistical properties [29]. In particular, the 1-point probability distribution function method [30] (`1pPDF`) fits the contribution of diffuse and PS components to the γ-ray 1-point fluctuations histogram. Employing `1pPDF` on Fermi-LAT data, it was possible to measure the PS count distribution per unit flux, dN/dS, below the LAT detection threshold at high latitudes [30–32], and to set competitive bounds on DM [33].

The scope of this Letter is to apply the `1pPDF` method to Fermi-LAT data from the IG to understand the role of faint PS to the GCE, while minimizing the mismodeling of diffuse emission components. To this end, we adopt a hybrid approach which combines, for the first time, adaptive template fitting methods as implemented in `skyFACT`, and `1pPDF` techniques.

Rationale, data, and methodology.—We follow a two-step procedure: first, we fit γ-ray data with `skyFACT` in order to build a model for the emission in the region of interest (ROI), maximally reducing residuals found to bias photon-count statistical methods [20]. Second, we run `1pPDF` fits with `skyFACT`-optimized diffuse models as input, and assess the role of PS to the GCE.

We analyze 639 weeks of `P8R3 ULTRACLEANVETO` Fermi-LAT data [34] until 2020-08-27. For the `skyFACT` fit, we consider an ROI of $40° \times 40°$ around the GC [35], and the 0.3–300 GeV energy range. We closely follow [12] and update the analysis for the increased data set and 4FGL catalog [36]. The emission model includes γ rays from inverse Compton scattering, π^0 decay, 4FGL pointlike and

 © 2021 American Physical Society

extended sources, the Fermi bubbles, the isotropic γ-ray background (IGRB), and the GCE. For the latter, we consider a template for the Galactic bulge emission as in [12], and one for a generalized NFW DM distribution with slope 1.26 (NFW126) [3,4]. We refer to [37] for more details.

We operate the 1pPDF analysis in the energy range 2–5 GeV [31,33], restricting to events with best angular reconstruction (evtype = PSF3) and coming from the inner $20° \times 20°$, IG ROI hereafter. We cut at latitudes $|b| > 0.5°$ or 2° to check the stability of 1pPDF results. The 1pPDF-fit model components are an IGRB template (free normalization), a diffuse emission template (free normalization), and an isotropic PS (IPS) [38] population with dN/dS defined by a multiple broken power law:

$$\frac{dN}{dS} = A_S \begin{cases} \left(\frac{S}{S_0}\right)^{-n_1} & S > S_{b1}; \\ \left(\frac{S_{b1}}{S_0}\right)^{-n_1+n_2}\left(\frac{S}{S_0}\right)^{-n_2} & S_{b2} < S \leq S_{b1}; \\ \vdots & \\ \left(\frac{S_{b1}}{S_0}\right)^{-n_1+n_2}\left(\frac{S_{b2}}{S_0}\right)^{-n_2+n_3}\cdots\left(\frac{S}{S_0}\right)^{-n_{N_b+1}} & S \leq S_{bN_b}. \end{cases} \tag{1}$$

The free parameters are A_S, the flux break positions, and the broken power-law indices, n_i [37]. The IPS dN/dS measured by the 1pPDF fit should recover the dN/dS of Fermi-LAT detected PS in the bright regime while pushing the PS detection threshold down to lower fluxes [30,31].

Our goal being to quantify the role of PS to the GCE within the 1pPDF, we add a *GCE smooth template* in the 1pPDF fit. As a baseline, we use the best-fit skyFACT bulge template in the 1pPDF fit (1pPDF-B), and we define the sF-B diffuse model as the sum of best-fit inverse Compton, π^0 decay, Fermi bubbles, and extended sources, thus subtracting the bulge emission. The normalization, $A_{B/\mathrm{NFW126}}$ for the bulge/NFW126 template, refers to the rescaling factor relative to the best-fit normalization from skyFACT.

On the one hand, the use of skyFACT best-fit diffuse model guarantees a robust characterization of GCE spectrum and morphology against systematics related to the mismodeling of the diffuse emission [3,20], resolving oversubtraction and undersubtraction issues by including a large number of nuisance parameters. The limitations of such a systematic uncertainty are indeed also relevant for the reconstruction of faint PS with 1pPDF methods [37]. On the other hand, the skyFACT optimization procedure mitigates possible systematics related to the mismodeling of unaccounted components [18], by allowing spatial remodulation in the fit templates. Also, we stress that this is the first time the stellar distribution in the Galactic bulge as tracer of GCE photons is used in pixel count statistical analyses (except for brief cross-checks, as in, e.g., [17]).

Besides the bulge, we also consider NFW126 as smooth GCE in the 1pPDF analysis (1pPDF-NFW126). In this case, we construct the corresponding skyFACT-optimized diffuse model (sF-NFW126) from the skyFACT run adopting NFW126 as GCE, in analogy with the sF-B model. Such a procedure guarantees maximal consistency between GCE and diffuse models adopted as input in the 1pPDF. Finally, to bracket the uncertainties related to the optimization of the diffuse model, we also build a skyFACT-optimized diffuse template from the skyFACT run not including any GCE additional template (sF-noGCE).

Results.—Our updated analysis of Fermi-LAT data with skyFACT confirms previous findings from [12–14]. A bulge distribution for GCE photons is strongly preferred by data on top of the NFW126-only model ($\sim 10\sigma$), and there is mild evidence for an additional NFW126 contribution on top of the bulge-only model ($\sim 4\sigma$), cf. [37]. This implies that the model maximally reducing the residuals is the skyFACT best fit of the run with the bulge.

We then use skyFACT-optimized diffuse and smooth GCE templates as input for 1pPDF fits, testing 0.5° and 2° latitude cuts. Our results are summarized in Fig. 1, where we show the best-fit dN/dS for the IPS in the IG ROI for several 1pPDF fit configurations. First, we notice that whatever GCE template is added to the 1pPDF fit components (bulge or NFW126), its normalization never converges toward the lower bound of its prior interval, regardless of the skyFACT diffuse template adopted. The same is valid for the IPS normalization. In all fit setups shown, an IPS population is recovered below the LAT flux threshold. The reconstructed IPS dN/dS is stable against systematics related to the choice of skyFACT-optimized diffuse template, and latitude cut. Moreover, it does not present any spurious effect at the Fermi-LAT threshold ($\sim 10^{-10}$ ph cm^{-2} s^{-1}), and IPS are resolved down to $\sim 10^{-11}$ ph cm^{-2} s^{-1} for $|b| > 0.5°$, depending on the modeling of the smooth GCE component. This holds true even when no GCE smooth template is included neither in the skyFACT fit nor in the 1pPDF one, contrary to what happens using nonoptimized diffuse models [18,20]. We therefore demonstrate, also in the context of 1pPDF methods, that reducing large-scale residuals from

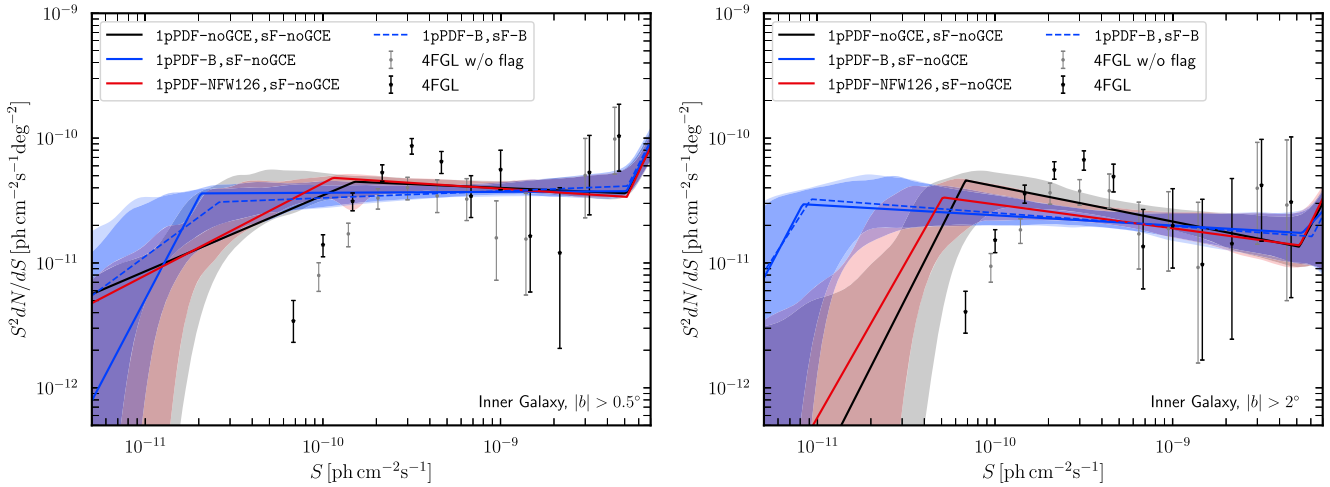

FIG. 1. IPS source count distribution in the IG ROI from the 1pPDF fit for $|b| > 0.5°$ (left) or 2° (right). Solid (dashed) lines correspond to sF-noGCE (sF-B) diffuse template. The black line illustrates the 1pPDF-noGCE case. The blue (red) line refers to the 1pPDF-B (1pPDF-NFW126) case. The colored areas correspond to 1σ uncertainty bands. The black (gray) points represent the count distribution of 4FGL sources (without any analysis flag, see [36]).

mismodeling of the diffuse emission improves the reconstruction of PS dN/dS (see also [37]). The reconstructed dN/dS has a normalization decreasing with increasing latitude cuts, suggesting that PS are more numerous toward the very GC. When an NFW126 template is included in the 1pPDF fit, the IPS dN/dS is compatible with the 1pPDF-noGCE case. In both cases, the second break in the dN/dS—in addition to the one set in the bright regime—is recovered close to the LAT flux threshold. Instead, the 1pPDF-B reconstructs PS down to lower fluxes, regardless of sF-noGCE or sF-B diffuse models. For these setups, the second flux break is found at $\sim 2 \times 10^{-11} (8 \times 10^{-12})$ ph cm^{-2} s^{-1} for $|b| > 0.5°(2°)$. Going from $|b| > 0.5°$ to $|b| > 2°$, the dN/dS is resolved down to even lower fluxes. *A posteriori*, we associate such a better sensitivity to IPS to the ability of the fitted diffuse components to further reduce fit residuals.

We quantify now the evidence for models with an additional smooth GCE template. To this end, we compare the global evidence, $\ln \mathcal{Z}$, for the 1pPDF-noGCE, 1pPDF-B, and 1pPDF-NFW126 setups, with different skyFACT diffuse model inputs. For each model combination, we compute the Bayes factor between model i and j, $B_{ij} = \exp(\ln \mathcal{Z}_i - \ln \mathcal{Z}_j)$, and assess the strength of evidence of model i with respect to model j. Our results are presented in Table I. Regardless of the skyFACT-optimized diffuse template adopted, data *always* more strongly support models which include an additional smooth template for the bulge with respect to models without GCE in the skyFACT and/or 1pPDF fits

TABLE I. Results for the 1pPDF analysis of the IG LAT data. First four columns: setup of the analysis and latitude mask of the IG. The $\ln(\mathcal{Z})$ is the nested sampling global log evidence extracted from Multinest [30]. Last two columns: flux percentage of different model components with respect to the total emission in the ROI (for $S < 10^{-8}$ ph cm^{-2} s^{-1}, see [37]), and normalization of smooth GCE template in the 1pPDF. Flux percentage always sum to unity within errors.

Description	1pPDF setup	skyFACT diffuse	$\lvert b\rvert$ cut [°]	$\ln(\mathcal{Z})$	Point sources/diffuse/GCE%	$A_{B/\mathrm{NFW126}}$
No GCE (both)	1pPDF-noGCE	sF-noGCE	2	−6113	12/89/−	⋯
Bulge (1pPDF only)	1pPDF-B	sF-noGCE	2	−6076	13/81/7	0.8 ± 0.1
DM (1pPDF only)	1pPDF-NFW126	sF-noGCE	2	−6084	10/84/6	$1.8^{+0.4}_{-0.2}$
Bulge (skyFACT only)	1pPDF-noGCE	sF-B	2	−6169	11/89/−	⋯
Bulge (both)	1pPDF-B	sF-B	2	−6074	13/77/10	1.1 ± 0.1
DM (both)	1pPDF-NFW126	sF-NFW126	2	−6084	11/82/7	2.3 ± 0.3
No GCE (both)	1pPDF-noGCE	sF-noGCE	0.5	−7822	13/86/−	⋯
Bulge (1pPDF only)	1pPDF-B	sF-noGCE	0.5	−7802	14/83/3	0.3 ± 0.1
DM (1pPDF only)	1pPDF-NFW126	sF-noGCE	0.5	−7818	14/85/1	0.3 ± 0.1
Bulge (skyFACT only)	1pPDF-noGCE	sF-B	0.5	−7907	15/85/−	⋯
Bulge (both)	1pPDF-B	sF-B	0.5	−7796	14/79/7	0.8 ± 0.1
DM (both)	1pPDF-NFW126	sF-NFW126	0.5	−7820	14/84/2	0.6 ± 0.2

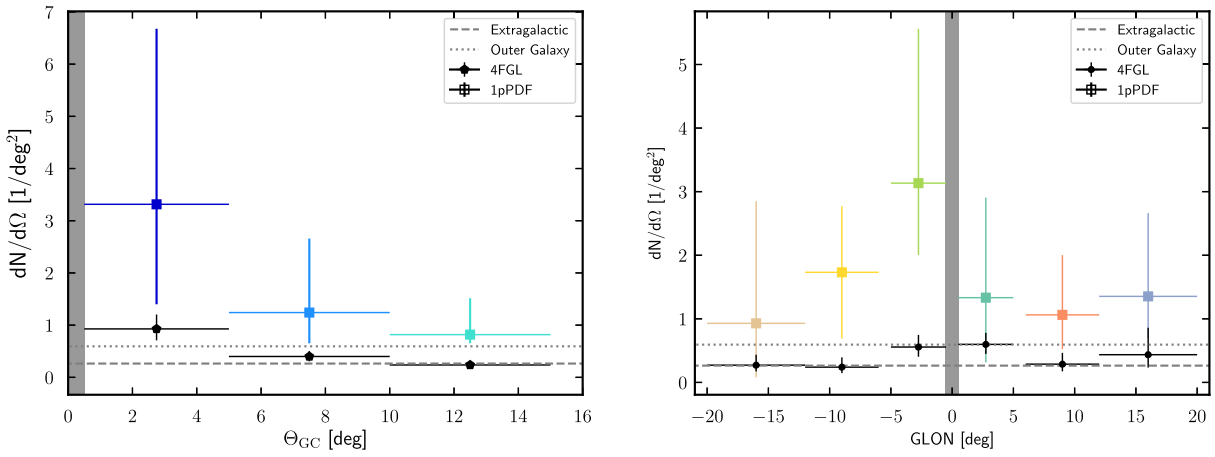

FIG. 2. Radial (left) and longitude (right) source density $dN/d\Omega$ profiles, as reconstructed by the `1pPDF-B` fit using the `sF-B` diffuse model. We also display source density profiles for 4FGL sources (black points), and average source densities in the OG and EG ROIs.

($\ln B_{ij} > 20$), *and* models with an additional smooth NFW126 component in the `skyFACT` and/or `1pPDF` fits ($\ln B_{ij} > 7$). Whenever a bulge template is included in our analysis, this is preferred even with respect to additional smooth DM templates. As for our baseline model, `sF-B`, and $|b| > 2°$, the evidence for an additional bulge template (`1pPDF-B`), with respect to `1pPDF-noGCE` is $\ln B \sim 95$. Moreover, in this case the normalization of the bulge template is $A_B = 1.1 \pm 0.1$, supporting the consistency between GCE and diffuse model adopted. This evidence is as strong also for $|b| > 0.5°$, $\ln B \sim 110$.

We note that, when we use the `sF-noGCE` diffuse model in the `1pPDF` fit including the bulge (`1pPDF-B`), we find comparable evidence to the `1pPDF-B`, `sF-B` setup. Indeed, `skyFACT` is able to reabsorb part of the photons from the bulge by remodulating (spatially) other diffuse templates, and so, partially reduces the residuals also in the `sF-noGCE` case. This is perfectly consistent with the fact that $A_B = 0.8 \pm 0.1$. Models with PS *and* a smooth bulge component are therefore strongly preferred by data, regardless of the optimized diffuse model employed. On the contrary, the evidence for an additional smooth NFW126 template with respect to models without GCE in the `skyFACT` fit and/or `1pPDF` fits depends on the choice of the `skyFACT`-optimized diffuse template adopted, as well as on the latitude cut.

We have tested our results against a number of systematic effects, which are detailed in [37].

The flux percentages reported in Table I illustrate that `1pPDF` fits to Fermi-LAT data find non-null (and even comparable) emission from both the IPS population *and* the smooth GCE template, in most cases each contributing about 10% of the total emission in the ROI. Since 4FGL sources (2° cut, without analysis flag, see Fig. 1) account for 7% (10% including flagged sources) of the total IG emission, the remaining flux comes from subthreshold IPS. We have verified [37] that our results are not driven by PS in the ultrafaint regime [19], where the sensitivity of the `1pPDF` method drops (as quantified by the magnitude of uncertainty bands in Fig. 1), and an IPS population may become degenerate with a truly diffuse emission.

We also measure the IPS dN/dS in two control regions: the outer Galaxy (OG, $|b| < 20°$, $60° < |l| < 90°$) and the extra-Galactic region (EG, $|b| > 40°$, $|l| > 90°$). The reconstructed dN/dS in both OG and EG ROIs does not present any spurious threshold effect and can identify IPS down to the statistical limit of the method around $\sim 10^{-11}$ ph cm^{-2} s^{-1} [30]. We compute the source density $dN/d\Omega$ in the flux interval $[10^{-11} - 10^{-9}]$ ph cm^{-2} s^{-1}, finding ~ 0.6 sources/deg^2 in the OG, and ~ 0.3 sources/deg^2 in the EG, see Fig. 2.

Since the spatial distribution of PS is *isotropic* by construction, we test the PS spatial behavior by dissecting the IG ROI into three concentric annuli, masked for latitudes $|b| < 0.5°$. We extract the dN/dS separately in each ring, and integrate it over the flux interval $[10^{-11} - 10^{-9}]$ ph cm^2 s^{-1}. The result is reported in Fig. 2 as a function of the mean $\Theta_{\rm GC} = \sqrt{b^2 + l^2}$ in each ring, for our baseline `1pPDF-B`, `sF-B` setup. We observe a decreasing trend of the $dN/d\Omega$ in the IG with $\Theta_{\rm GC}$. Also, the $dN/d\Omega$ in the innermost ring is about a factor of three higher than 4FGL sources, as well as than in OG and EG. For the most external ring, the source density is instead comparable with the catalog, OG and EG ones. This corroborates the evidence that the IG PS population is not purely isotropic nor extragalactic in origin, but rather it peaks toward the GC. Similarly, we build the longitude profile of IG PS, Fig. 2. The dN/dS has been fitted in six longitude slices from the GC bound at $|l| = 6°$, 12°, and 20°. The derived $dN/d\Omega$ shows again a distribution peaked around the GC, and compatible with OG (and partially with 4FGL and EG) sources only in the most external longitude interval. This result adds a piece of evidence that the GCE (defined as an excess of photons above traditionally

adopted foreground and background astrophysical models) is contributed by faint PS on lines-of-sight toward the Galactic Center, and, perhaps, in the Galactic bulge, supporting their *Galactic* origin.

Conclusions.—For the first time, we analyzed the IG Fermi-LAT sky by means of the `1pPDF` photon-count statistics technique in order to understand the role of PS to the GCE. To minimize the systematic effects inherent the modeling of the γ-ray sky, we introduced important methodological novelties. First, we implemented within the `1pPDF` new, *optimized*, models for the diffuse emission from `skyFACT` adaptive template fits, developing a self-consistent procedure which effectively reduces diffuse mismodeling. Second, besides PS, in the `1pPDF` fit we included an additional *smooth* GCE template which traces the stellar distribution in the Galactic bulge.

The updated `skyFACT` analysis of the IG confirms that the GCE is better described by a bulge template than an NFW126 model at high significance. Moreover, we find that the `1pPDF` method, supplied with `skyFACT` diffuse emission templates, always recovers an IPS population well below the Fermi-LAT flux threshold, down to $\sim 10^{-11}$ ph cm^{-2} s^{-1} for $|b| > 0.5°$. The reconstructed IPS dN/dS is stable against a number of systematics, in particular related to the choice of `skyFACT`-optimized diffuse template and latitude cut. Regardless of the `skyFACT`-optimized diffuse template, data *always* prefer models which include an additional smooth template for the bulge with respect to both models without it and models with an additional NFW126 template, in the `skyFACT` and/or `1pPDF` fits.

Our results show that, within the statistical validity of the `1pPDF` and the setups tested, IPS and diffuse bulge each contributes about $\mathcal{O}(10\%)$ to the γ-ray emission along the lines of sight toward the GC. In particular, within our baseline model the `1pPDF` founds that PS (bulge) contribute 13% (10%) of the total emission of the IG. Subtracting the contribution from cataloged sources, a non-negligible fraction of the IG emission is accounted by subthreshold PS. This further corroborates a possible, at least partial, stellar origin of the GCE.

We also verified that this IPS population is not purely isotropic nor extragalactic in origin, rather it peaks toward the very GC. Although the final confirmation of the PS nature of the GCE will most likely come from multi-wavelength future observations, we undoubtedly got one step closer to the understanding of the mysterious nature of the GCE emission.

We very kindly acknowledge the work formerly done by H. S. Zechlin on the `1pPDF` code. We warmly thank P. D. Serpico for inspiring discussion. We also thank M. Di Mauro, F. Kahlhoefer, M. Kraemer, P. D. Serpico, and C. Weniger for a careful reading of the manuscript and for insightful comments. The work of F. D. has been supported by the "Departments of Excellence 2018–2022" Grant awarded by the Italian Ministry of Education, University and Research (MIUR) (L. 232/2016). F. C. acknowledges support by the Programme National Hautes Energies (PNHE) through the Appel d'Offre Institut National Sciences de l'Univers (INSU) 2019, grant Dark matter subtructures in gamma rays ("DMSubG"), and the Agence Nationale de la Recherce Appel à projets générique 2019 AAPG2019, project Galactic emission from compact objects "GECO." S. M. acknowledges computing resources granted by RWTH Aachen University under Project No. rwth0578.

*calore@lapth.cnrs.fr
†donato@to.infn.it
‡manconi@physik.rwth-aachen.de

[1] K. N. Abazajian and M. Kaplinghat, Phys. Rev. D **86**, 083511 (2012).
[2] C. Gordon and O. Macias, Phys. Rev. D **88**, 083521 (2013); **89**, 049901(E) (2014).
[3] F. Calore, I. Cholis, and C. Weniger, J. Cosmol. Astropart. Phys. 03 (2015) 038.
[4] T. Daylan, D. P. Finkbeiner, D. Hooper, T. Linden, S. K. N. Portillo, N. L. Rodd, and T. R. Slatyer, Phys. Dark Universe **12**, 1 (2016).
[5] M. Ajello *et al.* (Fermi-LAT Collaboration), Astrophys. J. **819**, 44 (2016).
[6] J. F. Navarro, C. S. Frenk, and S. D. M. White, Astrophys. J. **490**, 493 (1997).
[7] F. Calore, I. Cholis, C. McCabe, and C. Weniger, Phys. Rev. D **91**, 063003 (2015).
[8] P. Agrawal, B. Batell, P. J. Fox, and R. Harnik, J. Cosmol. Astropart. Phys. 05 (2015) 011.
[9] S. Murgia, Annu. Rev. Nucl. Part. Sci. **70**, 455 (2020).
[10] M. Di Mauro, Phys. Rev. D **103**, 063029 (2021).
[11] K. N. Abazajian, J. Cosmol. Astropart. Phys. 03 (2011) 010.
[12] R. Bartels, E. Storm, C. Weniger, and F. Calore, Nat. Astron. **2**, 819 (2018).
[13] O. Macias, C. Gordon, R. M. Crocker, B. Coleman, D. Paterson, S. Horiuchi, and M. Pohl, Nat. Astron. **2**, 387 (2018).
[14] O. Macias, S. Horiuchi, M. Kaplinghat, C. Gordon, R. M. Crocker, and D. M. Nataf, J. Cosmol. Astropart. Phys. 09 (2019) 042.
[15] R. Bartels, S. Krishnamurthy, and C. Weniger, Phys. Rev. Lett. **116**, 051102 (2016).
[16] S. K. Lee, M. Lisanti, B. R. Safdi, T. R. Slatyer, and W. Xue, Phys. Rev. Lett. **116**, 051103 (2016).
[17] R. K. Leane and T. R. Slatyer, Phys. Rev. Lett. **123**, 241101 (2019).
[18] R. K. Leane and T. R. Slatyer, Phys. Rev. Lett. **125**, 121105 (2020).
[19] L. J. Chang, S. Mishra-Sharma, M. Lisanti, M. Buschmann, N. L. Rodd, and B. R. Safdi, Phys. Rev. D **101**, 023014 (2020).
[20] M. Buschmann, N. L. Rodd, B. R. Safdi, L. J. Chang, S. Mishra-Sharma, M. Lisanti, and O. Macias, Phys. Rev. D **102**, 023023 (2020).

[21] Y.-M. Zhong, S. D. McDermott, I. Cholis, and P. J. Fox, Phys. Rev. Lett. **124**, 231103 (2020).
[22] R. K. Leane and T. R. Slatyer, Phys. Rev. D **102**, 063019 (2020).
[23] S. Caron, G. A. Gómez-Vargas, L. Hendriks, and R. Ruiz de Austri, J. Cosmol. Astropart. Phys. 05 (2018) 058.
[24] F. List, N. L. Rodd, G. F. Lewis, and I. Bhat, Phys. Rev. Lett. **125**, 241102 (2020).
[25] F. Calore, M. Di Mauro, F. Donato, J. W. T. Hessels, and C. Weniger, Astrophys. J. **827**, 143 (2016).
[26] F. Calore, T. Regimbau, and P. D. Serpico, Phys. Rev. Lett. **122**, 081103 (2019).
[27] J. Berteaud, F. Calore, M. Clavel, P. D. Serpico, G. Dubus, and P.-O. Petrucci, Phys. Rev. D **104**, 043007 (2021).
[28] E. Storm, C. Weniger, and F. Calore, J. Cosmol. Astropart. Phys. 08 (2017) 022.
[29] D. Malyshev and D. W. Hogg, Astrophys. J. **738**, 181 (2011).
[30] H.-S. Zechlin, A. Cuoco, F. Donato, N. Fornengo, and A. Vittino, Astrophys. J. Suppl. Ser. **225**, 18 (2016).
[31] H.-S. Zechlin, A. Cuoco, F. Donato, N. Fornengo, and M. Regis, Astrophys. J. Lett. **826**, L31 (2016).
[32] S. Manconi, M. Korsmeier, F. Donato, N. Fornengo, M. Regis, and H. Zechlin, Phys. Rev. D **101**, 103026 (2020).
[33] H.-S. Zechlin, S. Manconi, and F. Donato, Phys. Rev. D **98**, 083022 (2018).
[34] Publicly available at https://heasarc.gsfc.nasa.gov/FTP/fermi/data/lat/weekly/photon/. More details are found at https://fermi.gsfc.nasa.gov/ssc/data/analysis/documentation/Cicerone/Cicerone_Data/LAT_DP.html.
[35] This ROI still allows us to discriminate the GCE morphology without suffering from systematics induced by selecting too narrow ROIs [14].
[36] S. Abdollahi *et al.* (Fermi-LAT Collaboration), Astrophys. J. Suppl. Ser. **247**, 33 (2020).
[37] See Supplemental Material at http://link.aps.org/supplemental/10.1103/PhysRevLett.127.161102 Sec. I for details on the SkyFACT analysis, Sec. II for details on the 1pPDF analysis, Secs. III–IV for systematic checks on the diffuse emission template and dN/dS modeling within the 1pPDF, and Sec. V for the dN/dS of the outer and extragalactic regions, which includes Refs. [39–47].
[38] As currently implemented, the `1pPDF` method does not allow to test spatially dependent dN/dS.
[39] S. Mishra-Sharma, N. L. Rodd, and B. R. Safdi, Astron. J. **153**, 253 (2017).
[40] K. M. Gorski, E. Hivon, A. J. Banday, B. D. Wandelt, F. K. Hansen, M. Reinecke, and M. Bartelmann, Astrophys. J. **622**, 759 (2005).
[41] F. Feroz, M. P. Hobson, and M. Bridges, Mon. Not. R. Astron. Soc. **398**, 1601 (2009).
[42] W. A. Rolke, A. M. López, and J. Conrad, Nucl. Instrum. Methods Phys. Res., Sect. A **551**, 493 (2005).
[43] F. Acero *et al.*, Astrophys. J. Suppl. Ser. **223**, 26 (2016).
[44] M. Ackermann *et al.*, Astrophys. J. **799**, 86 (2015).
[45] L. Maccione, C. Evoli, D. Gaggero, and D. Grasso, DRAGON: Galactic Cosmic Ray Diffusion Code (2011), ascl:1106.011, https://ui.adsabs.harvard.edu/abs/2011ascl.soft06011M/abstract.
[46] M. Ackermann *et al.* (Fermi-LAT Collaboration), Astrophys. J. **793**, 64 (2014).
[47] M. Ackermann and others, Astrophys. J. **750**, 3 (2012).